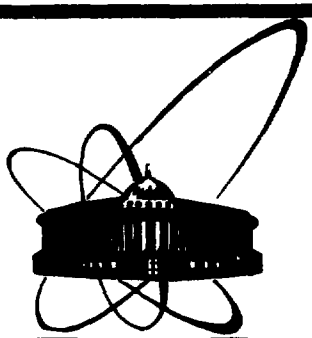

объединенный
институт
ядерных
исследований
дубна

E14-87-180

N.C.Popa

CORRECTION FOR THERMAL DIFFUSE SCATTERING IN THE TIME OF FLIGHT NEUTRON DIFFRACTION

Submitted to "physica status solidi"

1987

1. Introduction

Among the corrections necessary to find accurate structure factors from the diffraction measurements, the correction for thermal diffuse scattering (TDS) plays an important role. The diffractometer integrates the inelastic processes. If the result of this integration $I_T(s_1, s_2, s_3)$ is, in the neighbourhood of the Bragg peak, a monotonous function of the scan parameters s_i, the inelastic contribution can be substracted as a backround. But the backround subtraction eliminates only a part of the inelastic scattering if $I_T(s_1, s_2, s_3)$ is peak shaped. In fig. 1 is shown a diffraction peak obtained in a one-dimensional scan over the parameter s. The unhatched peak (I_B) is the Bragg scattering and the right hatched peak (I_T) is the TD scattering. The measured integrated intensity will be the area in the range $(-s_o, s_o)$ (the limits of the Bragg peak) minus the inelastic backround represented by the left hatched rectangle:

$$\mathcal{P} = \mathcal{P}_B + \mathcal{P}_T - \mathcal{P}_{Tb} = \mathcal{P}_B(1+\alpha) \qquad (1a)$$

$$\alpha = \frac{\mathcal{P}_T - \mathcal{P}_{Tb}}{\mathcal{P}_B} = \frac{1}{\mathcal{P}_B}\left[\int_{-s_o}^{s_o} I_T(s)\,ds - 2s_o I_T(s_o)\right]. \qquad (1b)$$

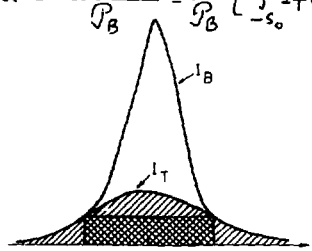

Fig. 1. Intensities measured in a one-dimensional scan in the neibourghood of the Bragg peak.

Here $\mathcal{P}_B$ and $\mathcal{P}_T$ are the Bragg and TDS integral intensities and α is the TDS correction. The index b means backround.

It is well known that only the one-phonon coherent scattering by low frequency acoustic modes produces a maximum $I_T(s)$ under the Bragg peak (see,e.g.,[1]). But taking into account only these modes it is possible to calculate the TDS correction *without a priori knowledge of the unit cell structure.* Only the elastic constants are necessary to know and these can be found by measuring the sound velocities along some directions in crystal. There are 3 constants for the cubic crystal, but 21 for the triclinic. But even for cubic crystals the exact calculation of α needs a long computer time because a multiple integral must be performed. The time is drastically reduced by using some approximations, the most important being the omission of the instrumental resolution, the high temperature of the *sample and the mean velocity approximation* [2,3] . The price which must be payed for, evaluated on some compounds by different authors, is 1% error in α for the first approximation [4] , 0.04% for the second one and $\lesssim$ 5% for the third [5] . In compensation, the correction α can be expressed by a third order integral which can be made analytically in a rough approximation (infinite vertical detector aperture [2]) or reduces to a double integral numericaly solved [3] .

The theory of the TDS correction initialy developed for X - rays was extended to the neutron diffraction. Here two different situations can be distinguished depending on whether the ratio β between the sound and neutron velocities is smaller or greater than unity [6,7] . In the first case the TDS correction is identical to that for the x - ray diffraction, but for $\beta > 1$ the quantity α decreases drastically with increasing β and could be even zero. The profile $I_T(s)$ in this

case was written for all the types of one-dimensional scans used in the angular dispersive (AD) method [8] but no quantitative analysis was provided up to now for the neutron time-of--flight (TOF) diffraction on monocrystals. In TOF were considered valid the conclusions found for the AD method [9]. In fact this is true only if the ratio ζ between the flight path after the sample and the total flight path is very small. Many diffractometers fulfil this condition but there are situations when ζ is near 1, like it is with the diffractometer for irradiated samples in Harwell [10]. In the general case TDS measured by TOF shows some peculiarities lost in the limiting case $\zeta \to 0$. These peculiarities were ignored in the paper of Cole & Windsor [11] which describes the basis of a program computing the TDS profile in the TOF diffraction on powders. This program uses less approximations but is time consuming and does not work for monocrystals. In the following a TDS correction formula for the TOF diffraction on monocrystals is found. Working for any TOF diffractometer this formula contains a function numericaly computable in a short time and two parameters which can be determined from the elastic constants or alternatively, in the refinement process together with the structure parameters.

2. TDS differential cross-section and the scattering surface

In the TOF diffraction the following differential cross--section [12] is measured:

$$\frac{d\sigma}{d\Omega} = \frac{L}{L_2} \int_{L_1^2 E_e / L^2} d E_1 \, \mathcal{F}(E_1, E_e) \left(\frac{E_1}{E_e}\right)^{3/2} \psi^{3/2}(E_1, E_e) \left(\frac{d^2\sigma}{d\Omega \, dE_2}\right)_{E_2 = \psi E_1} \qquad (2a)$$

$$\psi(E_1, E_e) = L_2^2 / (L\sqrt{E_1/E_e} - L_1)^2 . \qquad (2b)$$

where E_1, E_2 are the energies of the neutron before and after scattering, L_1, L_2 are the corresponding flight paths, $L = L_1 + L_2$

and E_e is the energy of the neutron elasticaly scattered. The factor $\mathcal{F}(\epsilon_1, E_e)$ takes into account the energy dependence of the incident flux, the absorbtion in sample and air and the detector efficiency; $\mathcal{F}(E_e, E_e) = 1$. The one-phonon cross-section of the acoustic modes which must be replaced in (2a) is [13] :

$$\frac{d^2\sigma}{d\Omega dE_2} = \frac{(2\pi)^3}{v_c} \frac{|F_{\underset{\sim}{Q}}|^2}{2M_c} \frac{K_2}{K_1} \sum_{j=1}^{3} \sum_{\underset{\sim}{\tau}}^{2.B.} \frac{|\underset{\sim}{Q}\,\underset{\sim}{\xi}_j(\underset{\sim}{q})|^2}{\omega_j(\underset{\sim}{q})}$$

$$\cdot \sum_{\varepsilon=\pm 1} \left\{ n[\omega_j(\underset{\sim}{q})] + \frac{1}{2} + \frac{\varepsilon}{2} \right\} \delta[\omega + \varepsilon\omega_j(\underset{\sim}{q})]\, \delta(\underset{\sim}{Q} - \underset{\sim}{H} - \underset{\sim}{q}) \qquad (3a)$$

$$\underset{\sim}{Q} = \underset{\sim}{K}_2 - \underset{\sim}{K}_1 \quad , \quad \hbar\omega = E_2 - E_1 , \qquad (3b,c)$$

where v_c and M_c are the unit cell volume and mass, $F_{\underset{\sim}{Q}}$ is the structure factor, $\underset{\sim}{H}$ is the reciprocal vector, $\underset{\sim}{K}_1$, $\underset{\sim}{K}_2$ are the wave vectors of the incident and scattered neutron, $\underset{\sim}{\xi}_j(\underset{\sim}{q})$, $\omega_j(\underset{\sim}{q})$ are the polarization vector and frequency of the mode $(j, \underset{\sim}{q})$; and $n(\omega)$, the Bose factor; the number ε is +1 and -1 for phonon creation and annihilation, respectively.

Firstly we performe the summation over $\underset{\sim}{q}$ in the Brilouin zone (Z.B. in (3a)) and further the integration over E_1 (in practice over K_1); as a result one obtains:

$$\frac{d\sigma}{d\Omega} = \frac{V}{v_c} |F_{\underset{\sim}{Q}}|^2 \frac{\hbar}{2M_c} \frac{L}{L_2} \sum_{j=1}^{3} \sum_{\varepsilon=\pm 1} \sum_{\nu} \mathcal{F} \frac{K_1^2}{K_2^2} \psi^2 \frac{|\underset{\sim}{Q}\,\underset{\sim}{\xi}_j(\underset{\sim}{q})|^2}{\omega_j(\underset{\sim}{q})}$$

$$\cdot \frac{n[\omega_j(\underset{\sim}{q})] + (\varepsilon+1)/2}{\left| 1 + \psi^{3/2} L_1/L_2 + m\varepsilon/\hbar K_1 \cdot (\underset{\sim}{i}_1 + \psi L_1/L_2 \cdot \underset{\sim}{i}_2)\, \nabla_{\underset{\sim}{q}} \omega_j(\underset{\sim}{q}) \right|} , \qquad (4)$$

where V is the sample volume, $\underset{\sim}{i}_1$, $\underset{\sim}{i}_2$ are the unit vectors along $\underset{\sim}{K}_1$ and $\underset{\sim}{K}_2$, respectively,

$$\underset{\sim}{q} = \underset{\sim}{Q} - \underset{\sim}{H} = \underset{\sim}{K}_2 - \underset{\sim}{K}_1 - \underset{\sim}{H} \qquad (5)$$

and K_1 are the roots of the following equation:

$$\kappa_1^2 \left[\psi(\kappa_1,\kappa_2) - 1\right] + 2m/\hbar \cdot \varepsilon\omega_j(\underset{\sim}{q}) = 0. \qquad (6)$$

The sum over τ in (4) means the sum over these roots. We are interested only in small $|\underset{\sim}{q}|$ (then $\underset{\sim}{Q}$ near $\underset{\sim}{H}$); in this case the dispersion relation is $\omega_j(\underset{\sim}{q}) = c_j(\underset{\sim}{q}/q)\,q$, c_j being the sound velocity in crystal, a quantity dependent on the acoustic wave direction and polarization. Now let us use the two velocities approximation [6] stating that all the acoustic waves are pure longitudinal and transversal (valid in fact only for some directions in crystal) with phase velocities c_1 (longitudinal) and c_2 (transversal) ($c_1 \neq c_2$) independent of direction. As a consequence $\nabla_{\underset{\sim}{q}}\omega_j(\underset{\sim}{q}) = c_j\,\underset{\sim}{q}/q$; on the other side the sum over $j = 1,3$ in (4) reduces to a sum of two terms, first being proportional to $|\underset{\sim}{Q}\,\underset{\sim}{\sigma}_1(\underset{\sim}{q})|^2 \simeq H^2\cos^2\varphi$ and the second one to $|\underset{\sim}{Q}\,\underset{\sim}{\sigma}_2(\underset{\sim}{q})|^2 + |\underset{\sim}{Q}\,\underset{\sim}{\sigma}_3(\underset{\sim}{q})|^2 = H^2\sin^2\varphi$, where φ is the angle between $\underset{\sim}{Q}$ and $\underset{\sim}{q}$. A more drastic approximation is $c_1 = c_2$ (full isotropy) and in this case the sum over j disappears. However, following Willis [6], a weaker approximation is prefered. In this approximation $c_1 \neq c_2$ but $\cos^2\varphi$ and $\sin^2\varphi$ are replaced by their averaged values 1/3 and 2/3, respectively. Other quantities in (4) also can be approximated; thus, by virtue of small energy transfer $\kappa_1 \simeq \kappa_2$ and consequently $\mathcal{F} \sim 1$. At last, for high temperature $\hbar\omega/\kappa_B T \ll 1$ which implies $n(\omega) = \left[\exp(\hbar\omega/\kappa_B T) - 1\right]^{-1} \simeq \kappa_B T/\hbar\omega \gg 1$, then we can neglect $(\varepsilon+1)/2$. In general this is valid for $T > T_D$ (T Debye), but for the low frequency acoustic waves it is valid also for $T < T_D$. The differential cross-section becomes:

$$\frac{d\sigma}{d\Omega} = \frac{V}{\tau_c}\,\frac{|F_{\underset{\sim}{H}}|^2 H^2}{2M_c}\,\frac{\kappa_B T}{3}\sum_{j=1}^{2}\frac{j}{c_j^2}\sum_{\tau}\sum_{\underset{\sim}{\xi}} q^{-2}\left|1 + \beta_j\,\varepsilon\left[\xi\,\underset{\sim}{i}_1 + (1-\xi)\,\underset{\sim}{i}_2\right]\frac{\underset{\sim}{q}}{q}\right|^{-1}, \qquad (7)$$

where we have denoted:

$$\xi = L_2 / L \cdot \quad , \quad \beta_j = c_j m / \hbar \kappa_{e0} = c_j / v_0 \qquad (8a,b)$$

Here κ_{e0} is κ_e which fulfils exactly the Bragg condition for the mean Bragg angle θ_B , and v_0 is the corresponding neutron velocity.

For the further calculations, the scattering surface given by the equations (5) and (6) must be investigated. Convenient handling can be done with

$$\varkappa = (\kappa_1 - \kappa_e) / \kappa_e \quad , \quad \gamma = (\kappa_e - \kappa_{e0}) / \kappa_{e0} \qquad (9a,b)$$

in place of κ_1 , κ_e . In the neighbourhood of the Bragg peak $\gamma \ll 1$; $\varkappa$ is also small; indeed, with (8a) and (9a), $\psi^{1/2} = \xi / (\varkappa + \xi)$ and since $\psi \simeq 1$, it results $\varkappa / \xi \ll 1$ and $\varkappa \ll 1$. As a consequence $\psi - 1 = (\psi^{1/2} + 1)(\psi^{1/2} - 1) \simeq -2\varkappa / \xi$ and the equation (6) becomes:

$$\gamma = \kappa_{e0} \xi \varkappa / \beta \xi . \qquad (10)$$

Thus for phonon creation $\varkappa > 0$ and conversely, $\varkappa < 0$ for phonon annihilation. To write down (5), let us denote by $\underset{\sim}{i}_{10}$, $\underset{\sim}{i}_{20}$ the unit vectors along the mean incident and diffracted beams, by $\underset{\sim}{\tau}_{20}$ the unit vector perpendicular to $\underset{\sim}{i}_{20}$ in the diffraction plane (see fig. 2) and $\underset{\sim}{\ell}_{20} = \underset{\sim}{i}_{20} \times \underset{\sim}{\tau}_{20}$. Neglecting

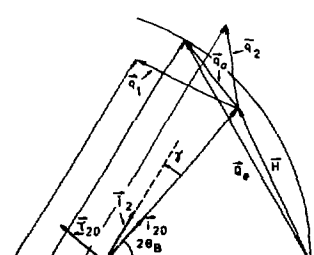

Fig. 2. The diagram of the scattering measured by the TOF diffraction. In a given direction (γ) and at the same TOF can be measured (if there are) an elastic process and inelastic processes with the wave-vector transfers $\underset{\sim}{Q}_e = \underset{\sim}{H} + \underset{\sim}{q}_e$ and, respectively, $\underset{\sim}{Q}_1 = \underset{\sim}{H} + \underset{\sim}{q}_1$ (phonon creation), $\underset{\sim}{Q}_2 = \underset{\sim}{H} + \underset{\sim}{q}_2$ (phonon annihilation).

the instrumental resolution (what allows us to write $\underset{\sim}{i}_1 = \underset{\sim}{i}_{10}$) and denoting by γ , δ the angular divergences of $\underset{\sim}{i}_2$ with respect to $\underset{\sim}{i}_{20}$ in and perpendicular to the diffraction plane, (5) becomes:

$$\underset{\sim}{q} = \kappa_{e0}\left[(\varkappa+y-\varkappa/\xi)\underset{\sim}{i}_{20} + \gamma\,\underset{\sim}{z}_{20} + \delta\,\underset{\sim}{l}_{20} - (\varkappa+y)\,\underset{\sim}{i}_{10}\right]. \quad (11)$$

By equalizing q^2 from (10) and (11) one obtains:

$$\left(\nu^2 - 1/\beta^2\right)\varkappa^2 - 2\xi M\varkappa + \xi^2 N^2 = 0, \quad (12)$$

where the following notations are used:

$$M = 2(\eta - \cos^2\theta_B)\,y - \zeta\gamma \quad (13a)$$

$$N^2 = 4y^2\sin^4\theta_B + (\gamma + y\sin 2\theta_B)^2 + \delta^2 \quad (13b)$$

$$\eta = 1 - 2\xi\sin^2\theta_B\,,\quad \zeta = \xi\sin 2\theta_B\,,\quad \nu^2 = \eta^2 + \zeta^2. \quad (14a,b,c)$$

For a given y the equation (12) represents, depending on the value of β , a rotational hyperboloid of two sheets or a rotational ellipsoid. The particular β values

$$\beta^{(1)} = 1/\nu\,,\quad \beta^{(2)} = 1/|\eta|\,,\quad (1 < \beta^{(1)} < \beta^{(2)}) \quad (15a,b)$$

define three regions for β . In the first region $(0 < \beta < \beta^{(1)})$ the equation (12) has one positive and one negative root for any γ and δ . The scattering surface is a hyperboloid of two sheets, one inside the Ewald sphere ($\varkappa > 0$ - phonon creation) and the second one outside ($\varkappa < 0$ - phonon annihilation). In the second region ($\beta^{(1)} < \beta < \beta^{(2)}$) the roots $\varkappa_1, \varkappa_2$ of (12) exist for any δ , but only for $\gamma \leq \gamma_1$ and $\gamma \geq \gamma_2$ where γ_1 , γ_2 are:

$$\gamma_{1,2} = \frac{-y\sin 2\theta_B(1-\beta^2\eta) \mp \sqrt{(\beta^2\nu^2-1)\left[4\sin^4\theta_B y^2 + (1-\beta^2\eta^2)\delta^2\right]}}{1-\beta^2\eta^2} \quad (16)$$

For $\gamma \leq \gamma_1$ both solutions $\varkappa_1$, $\varkappa_2$ are positive, and on the

contrary, are negative for $\gamma \geqslant \gamma_2$. Like in the first region the scattering surface is a hyperboloid of two sheets, inside and outside the Ewald sphere, but the angle of the asymptotic cone is acute and the rotation axis is inclined enough to give rise to a forbidden region in γ, where no TDS occurs. In the third region ($\beta > \beta^{(2)}$) the equation (12) has roots only for $\gamma_1 \leqslant \gamma \leqslant \gamma_2$ and $\delta^2 \leqslant 4 \sin^4\theta_B \, y^2(\beta^2\eta^2 - 1)$. The roots have the sign of M; the scattering surface is an ellipsoid inside or outside the Ewald sphere. In fig. 3 are displayed the scattering surfaces for the three regions of β and two values $y > 0$; for $y < 0$ they pass into the configuration obtained by inverting the figure with respect to the origin.

The main difference (concerning TDS) between the TOF and AD method is the existence of three distinct regions of β in the former, comparatively with two regions in the latter. If ξ is not very small, the location and extension of these regions are θ_B dependent. Remarkable also is the angle in the scattering plane ($\delta = 0$) between the rotation axis of the scattering surface and the normal to the Ewald sphere (approximated in fig. 3 by the plane $x = 0$):

$$\chi = 0.5 \, \mathrm{arctg}\left[-2\xi\zeta / (\nu^2 - \xi^2 - 1/\beta^2)\right]. \qquad (17)$$

If $\xi \to 0$, then $\eta \to 1$, $\zeta \to 0$, $\chi \to 0$ and $\beta^{(2)} \to \beta^{(1)} \to 1$; hence the second region disappears and TDS differential cross-section measured by TOF becomes identical with that measured by the AD method.

With the roots x_1 , x_2 once found, it is now possible to sum over τ and ε in (7). As ε is just the sign of $x_{1,2}$, the sum has, in fact, only two terms. In the region (1) of β the result will be proportional to N^{-2}. But $K_{20}N$ is just the module of the vector $\underset{\sim}{2}$ with the end on the Ewald sphere

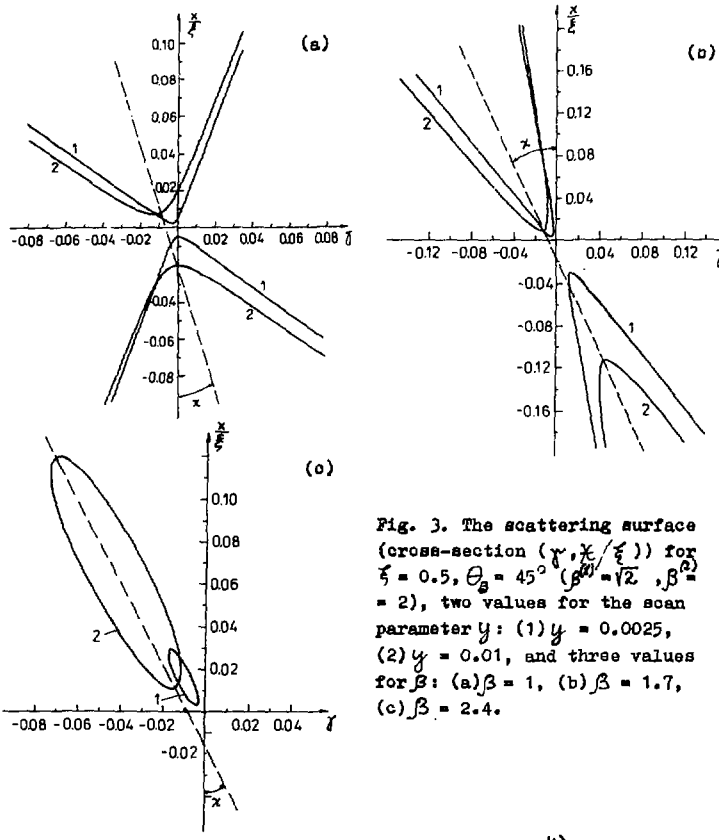

Fig. 3. The scattering surface (cross-section $(\gamma, \chi/\xi)$) for $\xi = 0.5$, $\theta_B = 45°$ ($\beta^{(1)} = \sqrt{2}$, $\beta^{(2)} = 2$), two values for the scan parameter y: (1) $y = 0.0025$, (2) $y = 0.01$, and three values for β: (a) $\beta = 1$, (b) $\beta = 1.7$, (c) $\beta = 2.4$.

(can be seen making $x = 0$ in (11)). Thus for $\beta < \beta^{(1)}$ the TDS differential cross-section measured by TOF is similar to the cross-section measured in AD method for $\beta < 1$. The structure of N suggests us to define the orthogonal coordinates (u, v, δ) in place of (y, γ, δ) for to determine a point in the neighbourhood of a lattice node:

$$u = 2y \sin^2\theta_B \quad , \quad v = \gamma + y \sin 2\theta_B \cdot \qquad (18a,b)$$

In these new coordinates the TDS differential cross-section is:

$$\frac{d\sigma}{d\Omega} = \frac{V}{v_c} \frac{|F_H|^2 H^2}{M_c} \frac{k_B T}{3 K_{e0}^2} \sum_{j=1}^{2} \frac{j}{c_j^2} F_j(u,v,\delta), \quad (19)$$

where

$$F_j(u,v,\delta) = 1/(u^2+v^2+\delta^2) \qquad \text{for} \quad \beta_j \le \beta^{(1)} \quad (20a)$$

$$F_j(u,v,\delta) = \frac{\beta_j z_{2(3)} (\eta u - \zeta v)}{(u^2+v^2+\delta^2)\sqrt{(1-\beta_j^2\eta^2)(v-v_1)(v-v_2)}} \quad \text{for} \quad \beta_j > \beta^{(1)}. \quad (20b)$$

The values v_1 , v_2 are obtained by (18b) from β_1 , β_2 ; the constants z_2 , z_3 corresponding to the second and the third region are:

$$z_2 = 1 \ (v \le v_1), \ z_2 = 0 \ (v_1 < v < v_2), \ z_2 = -1 \ (v \ge v_2) \quad (20c)$$

$$z_3 = \mathrm{sign}(\eta u) \ (v_1 \le v \le v_2), \ z_3 = 0 \ (v < v_1 , v > v_2). \quad (20d)$$

3. TDS correction for monocrystals.

For the TOF diffraction on monocrystals the parameter S of the commonly used one-dimensional scan is the time-of-flight or the wavelength $\Delta\lambda_e$. Let us denote by $2\Delta\lambda_0$ the range of the $\Delta\lambda_e$ scan and by $(2\gamma_0, 2\delta_0)$ the aperture of the detector with rectangular window. The three-dimensional window $2(\Delta\lambda_0, \gamma_0, \delta_0)$ is taken so large to see wholy the Bragg peak. Ignoring the resolution, the TDS profile for this scan is:

$$I_T(\Delta\lambda_e) = \iint_{\mathcal{D}(\Delta\lambda_e, \gamma_0, \delta_0)} d\gamma \, d\delta \ \frac{d\sigma}{d\Omega}(\Delta\lambda_e, \gamma, \delta), \quad (21)$$

where the integration domain $\mathcal{D}$ is the intersection (common area) between the detector window and the definition domain of the integrand. In the region (2) and (3) of β the latter depends on the scan parameter. Introducing (21) in (16) and taking account of (9b), (18) and of $\mathcal{P}_B = V|F_H|^2 \lambda_{e0}^4 / 2 v_c^2 \sin^2\theta_B$, one obtains:

$$\alpha = \frac{v_e}{(2\bar{v})^3}\,\kappa_{e0}\,\frac{H^2}{M_c}\,\frac{\kappa_B T}{3}\sum_{j=1}^{2}\frac{j}{e_j^2}\,\varphi\left(\beta_j, \theta_B, u_0, \gamma_0, \delta_0\right). \quad (22)$$

Here the following notations were used:

$$u_0 = 2\gamma_0 \sin^2\theta_B = 2\sin^2\theta_B\,\Delta\lambda_0 / \lambda_{e0} \quad (23)$$

$$\varphi = 2\int_0^{u_0} I(u)\,du - 2u_0\,I(u_0) \quad (24)$$

$$I(u) = \iint_{\Omega(u,\gamma_0,\delta_0)} d\delta\,d\nu\;F_j(u,\nu,\delta). \quad (25)$$

In the first region of β, Ω is given exclusively by the detector's window. Using (20a) for F_j, the integral over in (25) can be performed and the result is:

$$I^{(1)}(u) = 2\int_0^{\delta_0} d\delta\,\frac{1}{\sqrt{u^2+\delta^2}}\left[\operatorname{arctg}\frac{\gamma_0 + u\,\mathrm{ctg}\,\theta_B}{\sqrt{u^2+\delta^2}} + \operatorname{arctg}\frac{\gamma_0 - u\,\mathrm{ctg}\,\theta_B}{\sqrt{u^2+\delta^2}}\right]. \quad (26)$$

This integral can be performed only numericaly. For $u \to 0$ $I^{(1)}(u) \to \infty$, but this singularity is an integrable one.

In the region (2) and (3) of β the profile $I(u)$ has discontinuity points for derivatives. They are those points where the geometry of Ω changes. For example, in the region (2) one or other or the two sheets of the hyperboloid can be seen by the detector's window; in the region (3) the ellipsoid can be seen totally or partially. Thus, two discontinuity points are obtained equalizing γ_1 and γ_2 with $\pm\gamma_0$:

$$u_1 = |\beta^2\eta^2 - 1|\,\gamma_0 / \left(|1-\beta^2\eta|\,\mathrm{ctg}\,\theta_B + \sqrt{\beta^2\nu^2 - 1}\right) \quad (27a)$$

$$u_2 = |\beta^2\eta^2 - 1|\,\gamma_0 / \left(|1-\beta^2\eta|\,\mathrm{ctg}\,\theta_B - \sqrt{\beta^2\nu^2 - 1}\right). \quad (27b)$$

In addition, for the region (3) there is the point

$$u_3 = (\beta^2\eta^2 - 1)\,\gamma_0\,\mathrm{tg}\,\theta_B / |1-\beta^2\eta| \quad (27c)$$

obtained by equalizing $(\gamma_1+\gamma_2)/2$ with $\pm\gamma_0$; always $u_1 < u_3 < u_2$.

The integral over dv in (25) can also be made analytically if the integrand (20b) is preliminary rationalised. The result of integration can be expressed by means of the following primitive:

$$\Phi(A,B,C,R,S,t) = 2\int dt\,(Rt+S)/(At^2+2Bt+C)$$

$$= \frac{1}{2}\,\frac{R/\sqrt{C}-S/\sqrt{A}}{\sqrt{2}\sqrt{\sqrt{AC}-B}}\,\ln\frac{\sqrt{A}\,t^2+\sqrt{2}\sqrt{\sqrt{AC}-B}\,t+\sqrt{C}}{\sqrt{A}\,t^2-\sqrt{2}\sqrt{\sqrt{AC}-B}\,t+\sqrt{C}} \tag{28}$$

$$+\,\frac{R/\sqrt{C}-S/\sqrt{A}}{\sqrt{2}\sqrt{\sqrt{AC}+B}}\,\operatorname{arctg}\frac{\sqrt{A}\,t^2-\sqrt{C}}{t\sqrt{2}\sqrt{\sqrt{AC}+B}}$$

where we denoted:

$$\left.\begin{aligned} A &= u^2+\delta^2+v_1^2 \quad , \quad B = u^2+\delta^2+v_2^2 \quad , \\ C &= u^2+\delta^2+v_1v_2 \quad , \quad R = \eta u-\zeta v_2 \quad , \quad S = \eta u-\zeta v_1 \end{aligned}\right\} \tag{29}$$

The TDS profile in the regions (2) and (3) then is (only for $u \geq 0$):

$$\left.\begin{aligned} I^{(2)}(u) &= I_1(u)+I_2(u) && \text{for} \quad 0\leq u\leq u_1 \\ I^{(2)}(u) &= \begin{cases} I_1(u) \text{ if } \beta^2\eta-1>0 \\ I_2(u) \text{ if } \beta^2\eta-1<0 \end{cases} && \text{for} \quad u_1<u<\infty \\ I^{(2)}(u) &= 0 \quad \text{if } |\beta^2\eta-1|\,\operatorname{ctg}\theta_B < \sqrt{\beta^2v^2-1} && \text{for} \quad u_2<u<\infty \end{aligned}\right\} \tag{30a}$$

$$I_1(u) = \frac{2\beta}{\sqrt{1-\beta^2\eta^2}}\int_0^{D_1(u)} d\delta\;\Phi(A,-B,C,-R,S,t)\Big|_{T_{01}}^{T_1}$$

$$T_{01} = \sqrt{\frac{\delta_2+\delta_0}{\delta_1+\delta_0}} \quad , \quad T_1 = \begin{cases} \infty & \text{if } \delta_1\leq\delta_0 \\ \sqrt{\dfrac{\delta_2-\delta_0}{\delta_1-\delta_0}} & \text{if } \delta_1>\delta_0 \end{cases} \tag{30b}$$

$$I_2(u) = \frac{2\beta}{\sqrt{1-\beta^2\eta^2}}\int_0^{D_2(u)} d\delta\;\Phi(C,-B,A,S,-R,t)\Big|_{T_{02}}^{T_2}$$

$$T_{02} = \sqrt{\frac{\delta_1-\delta_0}{\delta_2-\delta_0}} \quad , \quad T_2 = \begin{cases} \infty & \text{if } \delta_2\geq-\delta_0 \\ \sqrt{\dfrac{\delta_1+\delta_0}{\delta_2+\delta_0}} & \text{if } \delta_2<-\delta_0 \end{cases} \tag{30c}$$

$$D_{1,2}(u) = \min\left\{\delta_0 , \left[\frac{(\delta_0 \mp u\,\mathrm{ctg}\theta_B)^2 + u^2 - \beta^2(\eta\delta_0 \mp u\,\mathrm{ctg}\theta_B)^2}{\beta^2\vartheta^2 - 1}\right]^{1/2}\right\} \qquad (30d)$$

In contrast with $I^{(1)}(u)$ the profile $I^{(2)}(u)$ is finite for $u \to 0$.

$$I^{(3)}(u) = \frac{2\beta\,\mathrm{sign}\,\eta}{\sqrt{\beta^2\eta^2 - 1}} \int_0^{D(u)} d\delta\, \Phi(A,B,C,R,S,t)\Big|_{T_1}^{T_2} \quad \text{for } 0 \le u < \infty$$

$$T_1 = \begin{cases} 0 & \text{if } \vartheta_2 \le \vartheta_0 \\ \sqrt{\dfrac{\vartheta_2 - \vartheta_0}{\vartheta_0 - \vartheta_1}} & \text{if } \vartheta_2 > \vartheta_0 \end{cases} \qquad T_2 = \begin{cases} \infty & \text{if } \vartheta_1 \ge -\vartheta_0 \\ \sqrt{\dfrac{\vartheta_2 + \vartheta_0}{-\vartheta_0 - \vartheta_1}} & \text{if } \vartheta_1 < -\vartheta_0 \end{cases} \qquad (31a)$$

$$I^{(3)}(u) = 0 \quad \text{if } |1 - \beta^2\eta|\,\mathrm{ctg}\theta_B > \sqrt{\beta^2\vartheta^2 - 1} \quad \text{for } u_2 \le u < \infty$$

$$D(u) = \min\left(\delta_0 , u/\sqrt{\beta^2\eta^2 - 1}\right) \quad \text{if } 0 \le u \le u_3$$

$$D(u) = \min\left\{\delta_0 , \left[\frac{(\delta_0 - u\,\mathrm{ctg}\theta_B\,\mathrm{sign}\,\eta)^2 + u^2 - \beta^2(\eta\delta_0 - u\,\mathrm{ctg}\theta_B\,\mathrm{sign}\,\eta)^2}{\beta^2\vartheta^2 - 1}\right]^{1/2}\right\} \quad \text{if } u > u_3 \qquad (31b)$$

Like in the region (1), the integrals over $d\delta$ in (30) and (31) are computed numericaly.

The typical profiles for the three regions of β are displayed in fig. 4; they were computed using the same values for β as in fig. 3. Both $I^{(2)}$, $I^{(3)}$ are zero for $u > u_2$ and $I^{(3)}$ is constant for $u < u_1$. In general $I^{(3)}$ is independent of u for $u \le u_4$, where

$$u_4 = \min\left(u_1 , \delta_0\sqrt{\beta^2\eta^2 - 1}\right). \qquad (32)$$

Mathematicaly this can be shown by replacing the integration variable δ in (31a) by $u\delta'/\sqrt{\beta^2\eta^2 - 1}$. For $u \le u_4$ the ellipsoid (scattering surface in reg. (3)) is wholy seen in the detector's window. $I^{(3)}$ is constant because the ellipsoid volume tend to

zero when $u \to 0$, but the cross-section tends to infinity with the *same rate*. Since the profile $I^{(3)}$ *is constant*, it is evident that the TDS correction is zero if $u_0 \leq u_4$. For $\beta \gtrsim \beta^{(2)}$ this condition *cannot* be realized since u_4 is very small; but u_4 increases monotonicaly with β , and if

$$u_0 < u_4 (\beta = \infty) = |\eta| \, tg\theta_B \, \gamma_0 \qquad (33)$$

the function φ is zero for $\beta > \beta^{(3)}$, where:

$$\beta^{(3)} = max \left\{ \frac{1}{|\eta|} \sqrt{1 + \frac{u_0^2}{\delta_0^2}} \; , \sqrt{\frac{\nu^2 + 2pt + \sqrt{\nu^4 + 4p(t\nu^2 - p)}}{2p^2}} \right\} \qquad (34a)$$

$$p = \eta^2 \gamma_0 / u_0 - |\eta| \, ctg\theta_B \quad , \; t = \gamma_0 / u_0 - sign\eta \, ctg\theta_B . \qquad (34b,c)$$

If the condition (33) is not fulfilled $\beta^{(3)} = \infty$.

The function φ from (22) is computed by numerical integration; a two-dimensional gaussian grid of 225 points ensures a good accuracy for any region of β , with a small expediture of time. For illustration, the factor φ versus β is displayed in the fig. 5 for a given Bragg angle, detector window and scan range and for different values of ξ .

The averaged velocities c_1 , c_2 from (22) can be calculated in principle from the elastic constants. Alternatively, these velocities can be considered as *free parameters in the* structure refinement process. This can be done only if the factor φ is computed a priori as a function of two variables β and u_0 . Indeed, for a data set measured at a given Bragg angle, the detector aperture and the range of scan necessary to see wholy the Bragg peak are (neglecting the contribution to resolution of the sample dimensions and detector thickness):

$$\gamma_0 = 3 \sqrt{\sigma_{\delta_i}^2 + 4\eta_m^2} \quad , \; \delta_0 = 3 \sqrt{\sigma_{\delta_i}^2 + 4\eta_m^2 \sin^2\theta_B} \qquad (35a,b)$$

$$u_0 = 6 \sin^2\theta_B \sqrt{\sigma_t^2 / T_{e0}^2 + \eta_m^2 \, ctg^2\theta_B} . \qquad (35c)$$

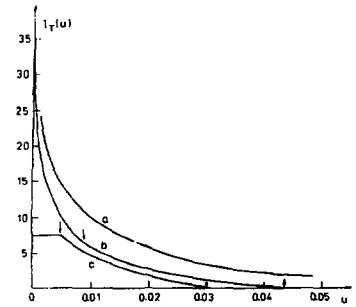

Fig. 4. The TDS profile $I(u)$ measured in the one-dimensional TOF scan for the detector aperture $\gamma_0 = 0.035$, $\delta_0 = 0.060$. a, b, c mean the first, second and third region of β. The values of ξ, Θ_B and β are the same as in fig. 2. The arrows show the points u_1 and u_2.

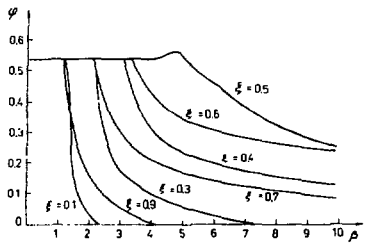

Fig. 5. The factor φ versus β for $\Theta_B = 75^0$, $u_0 = 0.05$, $\gamma_0 = 0.05$, $\delta_0 = 0.07$ and seven values for ξ.

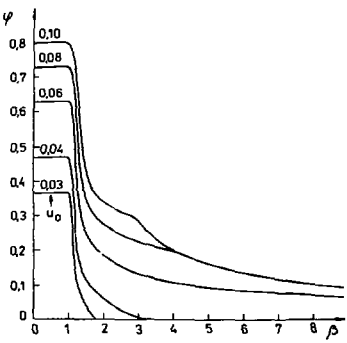

Fig. 6. The factor φ versus β for $\xi = 0.05$, $\Theta_B = 50^0$, $\gamma_0 = 0.05$, $\delta_0 = 0.07$ and five values for u_0.

Here η_m is the mosaic divergence of the sample $\sigma_{\xi_i}^2$, $\sigma_{\delta_i}^2$ are the dispersions of the angular distributions in the incident beam (in and perpendicular to the diffraction plane) σ_t^2 is the dispersion of its time distribution and T_{e0} is the TOF for the Bragg maximum. If the incident beam is formed by a neutron guide, σ_{ξ_i}, σ_{δ_i} have a weak dependence on λ but we can arrange to measure all the peaks (at a given Θ_B) with constant γ_0, δ_0. In general u_0 cannot be taken constant

in λ (except for $\sigma_t \sim \lambda$), therefore the factor φ must be computed a priori with both β and u_o variables. Hence it is obtained a two dimensional table (an exemple is given in fig. 6) from which the values of φ needed in the minimization process are extracted by interpolation.

It is a pleasure to acknowledge helpfull discussions with my collegue A.M.Balagurov.

References

[1] W.Cochran, Acta Cryst. A25, 95 (1969)

[2] N.Nilsson, Arkiv for Fysik, 12, 247 (1957)

[3] M.J.Cooper, K.D.Rouse, Acta Cryst. A24, 405 (1968)

[4] C.B.Walker, D.R.Chipman, Acta Cryst. A26, 447 (1970)

[5] E.F.Skelton, J.L.Katz, Acta Cryst. A25, 319 (1969)

[6] B.T.M.Willis, Acta Cryst. A25, 277 (1969)

[7] B.T.M.Willis, Acta Cryst. A26, 396 (1970)

[8] M.J.Cooper, Acta Cryst. A27, 148 (1971)

[9] B.T.M.Willis, Acta Cryst. A42, 188 (1986)

[10] C.G.Windsor, Pulsed Neutron Scattering, Taylor & Francis, London (1981)

[11] I.Cole, C.G.Windsor, Acta Cryst. A36, 697 (1980)

[12] A.M.Balagurov, A.I.Beskrovnii, N.Popa, Report J.I.N.R , P3-84-765, Dubna (1984) (in Russian)

[13] W.Marshall, S.W.Lovesey, Theory of Thermal Neutron Scattering, Oxford (1971)

Received by Publishing Department
on March 23, 1987.

Попа Н.К.

E14-87-180

Поправка на тепловое диффузное рассеяние в дифрактометрии по методу времени пролета

С использованием традиционных приближений вычислены поправки на тепловое диффузное рассеяние (ТДР) для случая дифракции нейтронов по методу времени пролета (МВП) на монокристаллах. Вклад ТДР в случае эксперимента по МВП будет отличаться от случая угло-дисперсивного метода измерения дифракции нейтронов, что может быть объяснено с помощью рассмотрения поверхности рассеяния. В случае МВП поверхность рассеяния имеет различные геометрии в трех областях отношений между скоростью звука в кристалле и скоростью нейтрона; в угло-дисперсивном методе имеются только две такие области. Различие между двумя методами измерения дифракции нейтронов исчезает, когда пролетное расстояние в случае МВП между образцом и детектором много меньше полного пролетного расстояния.

Работа выполнена в Лаборатории нейтронной физики ОИЯИ.

Препринт Объединенного института ядерных исследований. Дубна 1987

Popa N.C.

E14-87-180

Correction for Thermal Diffuse Scattering in the Time of Flight Neutron Diffraction

Using traditional approximations, the correction for thermal diffuse scattering in the neutron time-of-flight diffraction on monocrystals is calculated. This scattering measured by the time-of-flight method differs from that measured by the angular dispersive diffraction method and this can be explained with the aid of the scattering surface. In time-of-flight the scattering surface has different geometries in three regions of the ratio between the sound velocity in crystal and the neutron velocity; in the angular dispersive method there are only two such regions. The difference between the two methods disappears if the flight path after sample is very small comparatively with the total flight path.

The investigation has been performed at the Laboratory of Neutron Physics, JINR.

Preprint of the Joint Institute for Nuclear Research. Dubna 1987

18 коп.

Редактор Э.В.Ивашкевич. Макет Р.Д.Фоминой.

Подписано в печать 31.03.87.
Формат 60x90/16. Офсетная печать. Уч.-изд.листов 1,19.
Тираж 360. Заказ 38901.

Издательский отдел Объединенного института ядерных исследований.
Дубна Московской области.